Comprehensive study on the effects of fluid dynamics of air curtain and geometry, on infiltration rate of open refrigerated cavities

Mazyar Amin [a,*], Dana Dabiri [a], Homayun K. Navaz [b]

[a] Aeronautics and Astronautics Department, University of Washington, Seattle, WA 98195, USA
[b] Mechanical Engineering Department, Kettering University, 1700 University Ave., Flint, MI 48504, USA

ARTICLE INFO

ABSTRACT

To date, almost all the studies regarding the improvement of efficiency in open refrigerated display cases by improving the performance of air curtains have been limited to individual cases, which are usually specific to certain designs by certain manufacturers. This study targets the most important variables that can affect the infiltration associated with the entrainment and penetration of outside air into the system, and attempts to identify the relation between each of those variables and infiltration. Variables are defined in non-dimensional forms to make the problem independent from specific design, while each investigated variable covers a wide range of values. The refrigeration system has been eliminated and instead, a tracer gas technique has been employed for the measurement of infiltration. Infiltration results demonstrated a strong and direct relationship with the jet exit Reynolds number and offset angle. Although the relationship between infiltration and the other variables i.e. throw angle, height of the opening, and flow rate ratio, is very significant, the effect of each variable is better pictured in combination of the other variables.

© 2011 Elsevier Ltd. All rights reserved.

1. Introduction

Open type of Refrigerated Display Cases (ORDCs) are very popular in supermarkets all around the world to store the medium temperature products because they afford customers easy access to food products. In addition, the lack of doors eliminates the formation of a thin film of moisture deposited on the inner surface of the window glass after opening and closing the door for a few moments, which obscures visibility of the food products. Such advantages, of course, come with a high price: the penetration of the ambient air with higher energy content into the conditioned air inside the system causes mixing between these two airs. The undesirable result is an increase in the temperature of the food products. Consequently, the refrigeration system of ORDCs should deal with a greater cooling load, which will significantly increase the operating cost and also will deteriorate the food quality that may have health implications. Previous studies [1,2] indicated that up to 80 percent of the total cooling load of such systems is from air mixing. In recent decades, issuing an air curtain from one side of the opening of ORDCs, to achieve drastic reduction in the amount of

the mixing and lowering the associated cooling load during operating hours of supermarkets, has been more favored over using PVC stripes. Nonetheless, air curtains are not perfect and their performance very much depends on the geometrical configuration of display cases [3], flow dynamics of the air curtain jet at the nozzle exit [4,5], pressure difference across the air curtain [6,7], temperature difference between the discharged jet and ambient [8,9] as well as temperature difference between a room protected by a non-circulated air curtain [6], and the perturbation in the integrity of the curtain caused by the motion of the people around it, or even by flow current from the air conditioning systems of supermarkets. However, most studies on ORDCs, and particularly on the vertical types, ORVDCs have focused on systems with no, or only few variations in the geometry and characteristic flow dynamics associated with the systems. In order to better characterize the behavior of such air curtains on the infiltration rate of outside air into the return passage of the system, one ought to consider all the possible variables together, particularly those believed to have the greatest influence on the rate. Furthermore, each variable should span a relatively wide range of values. Recently, a series of extensive experimental investigations were embarked upon [10,11] to address the above concerns. Present work is in continuation of those works and emphasizes on some *primary* variables that can affect the infiltration rate most. The effect of another group of variables (called *secondary* variables) that are thought to be

---

* Corresponding author. Parks College of Engineering, St. Louis University, St. Louis, MO 63103, USA. Tel.: +1 206 931 7621/206 932 7621.
 E-mail addresses: mazyar@uw.edu, mamin2@slu.edu (M. Amin).

important, nevertheless are of less degree of importance compared to that of the *primary* variables, will be discussed in another article in the near future. The current work, assumes that imperfections that are usually, and inevitably, incorporated into ORDCs due to limitations in the design, manufacturing, and the improper usage of the systems in supermarkets, are not a consideration here. Every manufacturer, system and user has its own particular issues that cannot be easily dealt with in a research study. For instance, since the duct that is immediately located before the air curtain discharge typically experiences a right-angle turn, the velocity profile of the exit may be skewed along the width (the smaller edge) of the nozzle; therefore, this profile shape may be different from one designer to the other. Moreover, the formation of rather non-uniform flow along the length of the discharge owing to using a few axial fans is another example that may simply not be taken into account. To bypass these issues in the present work, a symmetric and fairly top-hat velocity profile across the jet exit width, which was also reproducible along the length of the discharge, was created by one long cross-flow fan.

The goal of this study is to present universal observations and results of infiltration rate of typical single band, multi-deck ORVDCs.

2. Problem description

2.1. Identification of important variables impacting infiltration

It should be noted that in an ORDC, the infiltrated air is either the entire outside air entrained by air curtain (seldom), or only a portion of it (often), that will be drawn into the return passage. In order to render an almost comprehensive set of data of infiltration in ORVDCs, it is critical to identify the variables that are believed to have the highest impact on the infiltration rate. Past studies [3,10,12] have listed up to total of nineteen variables (*primary + secondary*) and concluded that due to the enormous number of the combination of variables, it is unfeasible to take into consideration all the variables. However, they suggested a careful selection of a group of those variables. In another attempt to further reduce the number of variables, the non-dimensional forms of the variables were utilized. In this approach, first, the ranges of non-dimensional variables applicable to ORVDCs need to be determined. Then, upon using the non-dimensional form of the original variables, it will be sufficient to only vary one of the original variables that constitute the non-dimensional variable, rather all. This method will eliminate the difficulty associated with varying some of the variables. Furthermore, the obtained non-dimensional data from one ORVDC can be applicable to any ORVDC with different dimensions and flow characteristics as long as the values of the non-dimensional variables are retained and the geometrical and fluid dynamics of the problem are similar. The mass of infiltrated outside air ($\dot{m}_{Inf}$) into the system can be characterized as functions of some non-dimensional groups of *primary* and *secondary variables* shown in Eq. (1) [3]:

$$\frac{\dot{m}_{Inf}}{\dot{m}_{tot}} = f\left(\underbrace{\frac{H}{w}, \alpha, \beta, Re, \frac{\dot{m}_{BP}}{\dot{m}_{tot}}}_{\text{primary variables}}\right)$$
$$\times \underbrace{\Theta\left(\frac{T_{Am} - T_{DAG}}{T_{Am}}\right) \times \Omega(R.H.) \times \Phi(I_{DAG}) \times \Psi(F)}_{\text{functions of secondary variables}} \quad (1)$$

The other variables H, w, α, β, $\dot{m}_{BP}$, $\dot{m}_{tot}$ have been depicted in Fig. 1. The Reynolds number at the discharge air nozzle is defined as $Re = \dot{m}_{DAG}/(\mu w)$, where μ is the dynamic viscosity of air. T, $R.H.$, I,
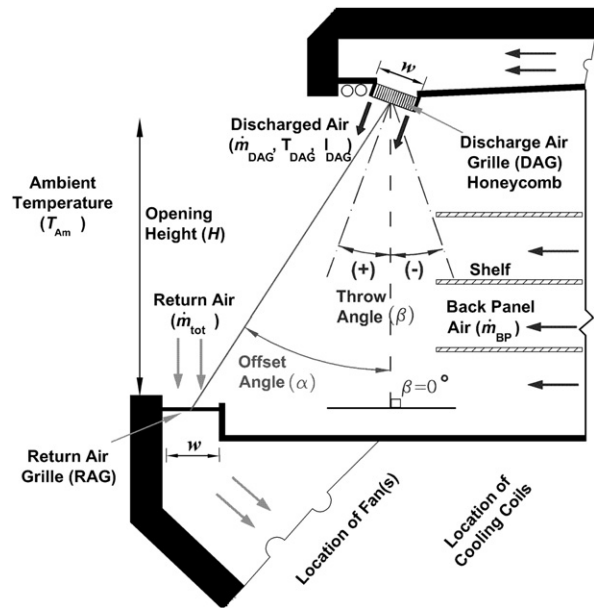

Fig. 1. Schematic of the side section of a typical ORVDC.

and F are temperature, relative humidity of ambient, turbulence intensity at the jet exit, and food level on shelves, respectively, and indices Am and DAG denote *ambient* air and *discharge* air at the jet nozzle exit. To be more specific, β (throw angle) is the angle relative to the vertical line that an air curtain jet leaves the discharge nozzle, and α (offset angle) represents the horizontal offset of the return air passage (RAG) relative to the discharge nozzle. In ORVDCs the total flow rate of the system, $\dot{m}_{tot}$, which enters the return passage, is divided into two flows, one discharging from the back panel and the other from the discharge at the top of the system that forms the air curtain; thus $\dot{m}_{tot} = \dot{m}_{RAG} = \dot{m}_{DAG} + \dot{m}_{BP}$.

This work focuses only on the effect of the *primary* variables and tries to experimentally establish or examine the effect of those variables on infiltration. The effect of the *secondary* variables will be discussed in a future work.

The values of non-dimensional *primary* variables of typical (or more common) ORVDCs, as well as the values of the variables tested in this study, have been presented in Table 1. This table along with Fig. 1 demonstrates that in this work the throw angle (β) takes both positive and negative values, while the offset angle (α) only takes positive values. Furthermore, it is evident from Table 1 that the selected values for this study span wide ranges, within which the values of the typical ORVDCs fall.

Hereafter, the ratio of $\frac{\dot{m}_{BP}}{\dot{m}_{tot}}$ will be denoted by K.

2.2. Experimental approach

2.2.1. Air curtain simulator

Using the values in Table 1, the total number of test cases resulting from the combination of the variables would be 576, making it too difficult and almost impractical to build as many custom-made ORVDCs. Therefore, an *air curtain simulator* (Fig. 2) was designed [10,12] to accommodate all the possible permutations. Before the air curtain jet is discharged, the simulator attenuates the turbulence of the flow by using air straighteners such as honeycombs, screens, and perforated plates, to produce a rather small turbulence (2.5% ± 1%) percent at the discharge nozzle. The reason for the choice of such small turbulence intensity was to

Table 1
Range of non-dimensional *primary* variables.

	H/w	Re_{DAG} (±200)	α	β	$\frac{\dot{m}_{BP}}{\dot{m}_{tot}} \pm 0.03$
Typical ORVDC	12	4000	0°	0°	0.4
Current study	8	Four values within the range	0°	−5°	0
	12	of [1600–8400] depending	16°	0°	0.35
	16	on the value of $\frac{\dot{m}_{BP}}{\dot{m}_{tot}}$	24°	5°	0.55
				13°	1

temporarily turn off the effect of turbulence because the ORVDC of each manufacturer is different from the others. In the future work, when investigating the *secondary* variables, the effect of higher values of turbulence intensity will be discussed. However, it was observed that the geometrical and fluid dynamic variations made to achieve the values of the *primary* variables in Table 1 have minimal effect (the above 1% standard deviation) on the amount of the turbulence intensity.

Knowing that the amount of infiltration in a typical ORVDC is almost independent of the difference between the temperatures of the discharged cold air and the ambient [13], and also considering the fact that the flow in the air curtain region is momentum-driven and the effect of buoyancy is relatively small in these systems [9], elimination of the refrigeration system could be very intriguing. Upon elimination of the refrigeration system, nevertheless, the two common methods of infiltration measurements, both of which are based on conservation of energy, i.e. collected condensate mass [13], and *thermal entrainment* [14], would not be applicable, and instead another method (tracer gas technique) should be proposed and employed. Reference [9] is a valuable work because it quantifies the effects of the Richardson Number, $Ri = Gr/Re^2$ (Ratio of Grashoff to the square of Reynolds number) on the entrainment. The buoyancy effects that are manifested by the Grashoff number will demonstrate a controlling role on the entrainment. It is found that for Reynolds number (based on the DAG width) of about 100 or less, the buoyancy forces become significant. The aforementioned conclusion of reference [13] and also results of the present work are obtained for Reynolds numbers with ranges significantly greater than $Re = 100$, making the assumption of insignificant buoyancy effect more appropriate.

2.2.2. Tracer gas technique

The application of tracer gas technique for measurement of infiltration in ORDCs, which is established on the conservation of

mass of an added tracer gas and air, discussed in details in reference [15]. This method can be used with or without a refrigeration system, but as was mentioned earlier the refrigeration system was not used in this research. In that work, they found that the results from the tracer gas technique have been shown to be in very good agreement with the other two energy methods mentioned above. They also discussed that the tracer gas tests can be performed faster and with higher accuracy. In addition, one can directly measure the amount of $\dot{m}_{tot}$ directly by tracer gas, instead of employing less accurate commercial anemometers or sophisticated and expensive laser-based techniques such as PIV (Particle Image Velocimetry) [9,13,16] or LDV (Laser Doppler Velocimetry) [12]. In the current work, carbon dioxide (CO_2) has been used as the tracer gas, and was released far in the upstream of the jet and subsequently was sampled at three zones: 1) before the jet exit (Fig. 2); 2) across the jet within the room (in a 1–1.5 m distance); and 3) in the downstream of the return passage. It was shown [15] that a non-dimensional infiltration rate (N.I.R.) can be expressed in terms of the concentration of tracer gas at the above three locations as:

$$N.I.R. = \frac{\dot{m}_{Inf}}{\dot{m}_{tot}} = \frac{C_{Dis} - C_{RAG}}{C_{Dis} - C_{Rm}} \qquad (2)$$

In this equation C denotes the mass concentration of the sampled tracer gas. It should be noted that C_{Dis} is the concentration of the mixture before the jet nozzle, and in this set up (Fig. 2) is also equal to that of the back panel flow. The concentration at the upstream of the discharge nozzle was kept between 20 000 and 25 000 ppm, with associated ambient concentration between 2500 and 4000 ppm. Each individual infiltration test could be carried out only in 20 min or less. C_{RAG} is the concentration measured after the inlet of the return passage in Eq. (2). Before the tests, CFD simulations (by Fluent software, ANSYS Co.) were performed [15] to identify the proper location of the sampling probes that are used to find the concentration of the gas across the air curtain and within the room (C_{Rm}).

3. Results and discussions

The infiltration results will be categorized and discussed in four sections based on the four $\frac{\dot{m}_{BP}}{\dot{m}_{tot}}$ ratios in Table 1. In the end, the results of different groups will be compared. This ratio takes four
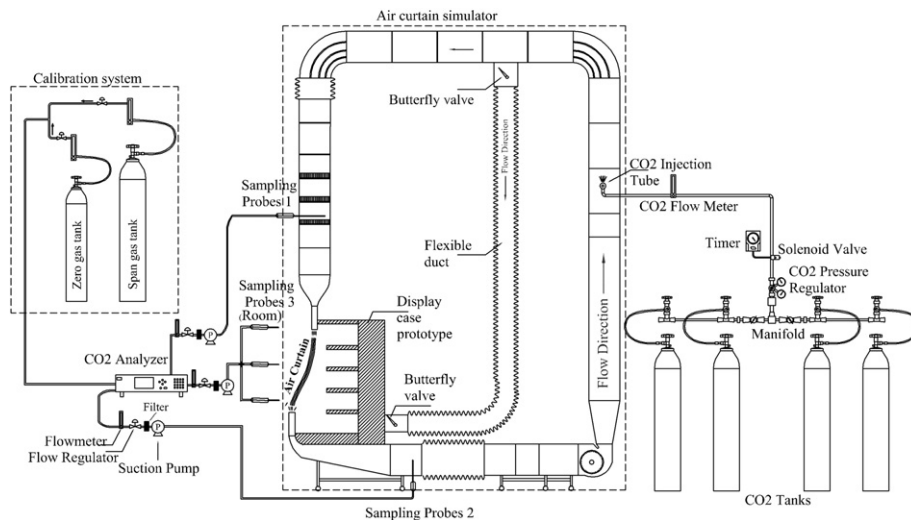

Fig. 2. Schematic of the side view of the air curtain simulator and infiltration measurement equipment.

values of 0, k_1, k_2, 1, where $k_1 = 0.35 \pm 0.03$ and $k_2 = 0.55 \pm 0.03$ are called *medium-low* and *medium-high* values of the back panel flow ratio, respectively. The variations of k_1 and k_2 are somewhat dependent on the Reynolds number at the air curtain discharge and geometrical configuration of the experimental set up.

Almost 576 data points were found to cover the range of levels of the primary variables presented in Table 1. Minimum and maximum values of the results have been presented for both absolute infiltration rate (which is specific to our air curtain simulator) and non-dimensional infiltration rate (which is universal among geometrically and fluid dynamically-similar display cases). The absolute infiltration rate of our air curtain simulator is smaller than a similar display case due to its smaller *Re*, but this fact does not diminish the merit of the absolute infiltration, and similar qualitative conclusions can be drawn for an actual similar display case by using the *N.I.R.*

3.1. Zero back panel cross flow

This section summarizes a past work [3], which is presented here for the sake of comparison with the results of the other ratios. In this case *K* is zero, which means that all the flow that is drawn by the *RAG* is supplied only through the *DAG*. In this configuration, the Reynolds numbers at the *DAG* were 2200, 3400, 5500, and 8400, with relatively small turbulence intensities of $2\% \pm 0.5\%$. It should be again emphasized that since the variables used in this work are in non-dimensional forms, the non-dimensional results can be generalized to any display case system regardless of size and total flow rate of the system, provided that the display case obtains non-dimensional variables that fall within the range of the variables in Table 1, i.e. the geometrical and fluid dynamic similarities are met. Due to the large volume of data generated by this work, only a selection of the data will be rendered.

The experimental results show the *absolute* value of infiltration rate ($\dot{m}_{Inf}$) in all test case scenarios increases with increase of the Reynolds number; Fig. 3 demonstrates the variation of infiltration with the Reynolds number in two different cases. In fact the higher the speed of the jet, the more the turbulence will be induced in the downstream of the jet exit. This in turn will enhance entrainment of ambient air into the air curtain jet as well as more mixing. Consequently, this will result in the ingress of a greater amount of ambient air into the system. The ambient air has a higher content of energy (sensitive and latent energy) than the air inside the display case compartment, which imposes more cooling load on the refrigeration of the ORVDCs. It is also evident from the figure that at smaller Reynolds numbers, the difference between the absolute infiltrations of different offset angles (α) will be smaller and the difference increases with an increase of the Reynolds number. Fig. 4 corresponds to the *N.I.R.* values of the data in Fig. 3.

Fig. 3 indicates that the absolute infiltration rate increases monotonically with increase of *Re*. On the other hand, however, the *N.I.R.* decreases when *Re* increases (Fig. 4). In fact, *N.I.R.* can be interpreted as the efficiency of an air curtain in entraining ambient air. The smaller *N.I.R.* a system has, the higher efficiency it will have, such that the smaller value of *N.I.R.* at a higher *Re* number infers that the air curtain is less capable of entraining and infiltrating ambient air, despite its higher momentum at the nozzle discharge. Perhaps the greater possibility of retaining the integrity of the air curtain jet at a higher Reynolds numbers, due to the greater momentum, is the main reason for this observation. Fig. 4 demonstrates that the rate of decrease of *N.I.R.* at smaller Reynolds numbers is greater than those at higher Reynolds numbers. Such behaviors seen for the absolute and non-dimensional infiltration rates, were seen in all test case scenarios. In addition in many cases the dependency of both absolute and non-dimensional
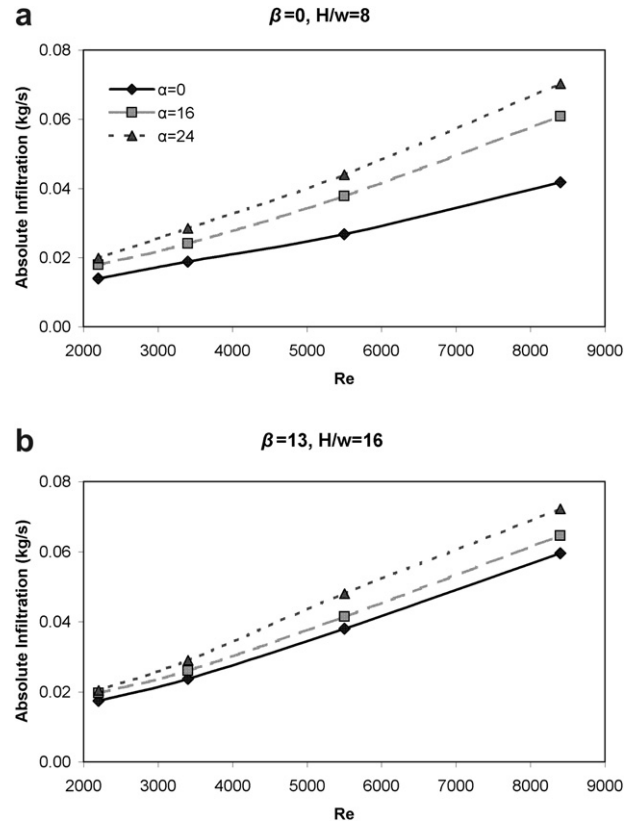
Fig. 3. Effects of the Reynolds number and offset angle on the *absolute* infiltration rate at different β and *H/w* values, and $K = 0$ [3].

infiltrations on offset angle was smaller at larger throw angles (β) (Fig. 5). This is more pronounced at smaller *H/w* ratios (e.g. $H/w = 8$) where the suction power of the return passage has stronger influence on the air curtain flow in that the jet can be more easily redirected toward the passage. Also, as Figs. 3 and 4 show, in most scenarios the absolute infiltration rate and *N.I.R.* increase with increase of α. The longer distance that air curtain flow travels from the discharge to the return at larger offset angles may be a factor in this change. Indeed, at longer distances, the jet loses more momentum before regains momentum by the suction power. Another factor that may have a role in the instability of the flow is its curved path that it undergoes on the way toward the return passage. Also one may adjust the discharge nozzle angle (β) to better direct the flow toward the return passage and consequently enhance the integrity of the air curtain. The above remarks imply that the effect of α on the infiltration is more substantial than that of β (because infiltration almost always increases with offset angle regardless of the values of throw angles, in the current range of the variables). In other words, α predominates β in affecting the infiltration rate. Increase of α can alter the development of the air curtain by impingement of the jet on the lowest horizontal surface of the display case and the subsequent upward agitated flow. The dependency of infiltration on α is almost linear in most cases as shown in Fig. 5. Similar trends were also seen in *N.I.R.*s.

From Fig. 5, it is obvious that that the infiltration depends on β as well. In almost all cases the smallest values of the throw angle for $K = 0$ (i.e. $\beta = -5°$) bring about the least amount of infiltration. In this case, the *N.I.R.* is characterized by similar behavior too. Nonetheless, both the absolute and non-dimensional infiltrations experience different trends of change with change of β. Previously mentioned that the minimum amount of infiltration at $K = 0$ always occur
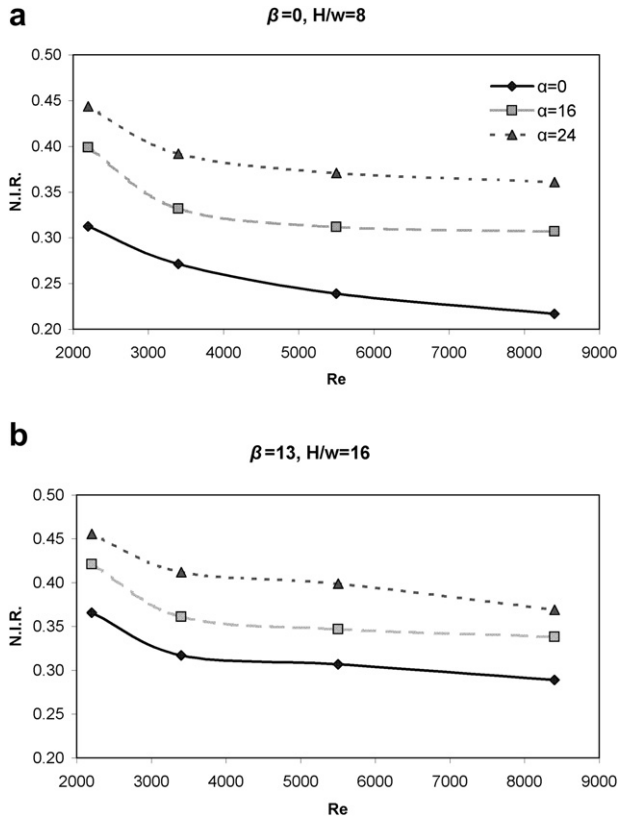
Fig. 4. Effects of the Reynolds number on the *N.I.R.* at *K* = 0 [3].

at $\beta = -5°$, but with increases of β from $-5°$ to $0°$ the infiltration usually increases and then decreases, or stays unchanged by $\beta = 5°$. Depending on the *H/w* ratio, with a further increase of β to greater values than $5°$, the infiltration may decrease, increase or stay constant (Fig. 6a and b). This variation is more pronounced at the smallest value of *H/w*, i.e. 8 (Fig. 6a). As a matter of fact, at *H/w* = 8, when β takes the largest value (i.e., $13°$), infiltrations of all α angles collapse and the dependency of infiltration on β is lost (Fig. 6a). In this figure at $\alpha = 0°$ the infiltration increases by increase of β from $5°$ to $13°$ because the nozzle directs the jet away from the return passage. On the other hand, infiltration reduces in the other two offset angles indicating that at larger α's there is a greater chance that the jet flow is directed toward the *RAG* (this may be observed only at *H/w* = 8). However, no significant changes in the pattern of variation of β at fixed α angles were seen when *Re* changed. Infiltration decreases at larger α and β angles, as is shown in Fig. 6a depicts, because when α increases, larger β can better aim the flow at the *RAG*.

In display cases, another factor that has been very prominent in affecting the amount of infiltration is the opening height. One may expect that with a change in *H* the curvature of the air curtain, which is also a function of α and β, will change again. With a change in *H/w*, infiltration rate altered with different trends; for instance at $\beta = -5°$ and *Re* = 2200, the infiltration rate experiences a valley at around *H/w* = 12 (Fig. 7a). If $\beta = -5°$ and *Re* = 5500 (Fig. 7b) the infiltration increases monotonically with increase of *H/w*.

In some other cases such as where $\beta = 13°$ and *Re* = 2200 (Fig. 7c), an increasing trend with a declining growth of infiltration was noticed when *H/w* increases On the other hand, Fig. 7d shows a case that gathers all the above patterns when offset angle varies. Therefore, the offset angle is one of the important factors that should be considered when determining opening height.
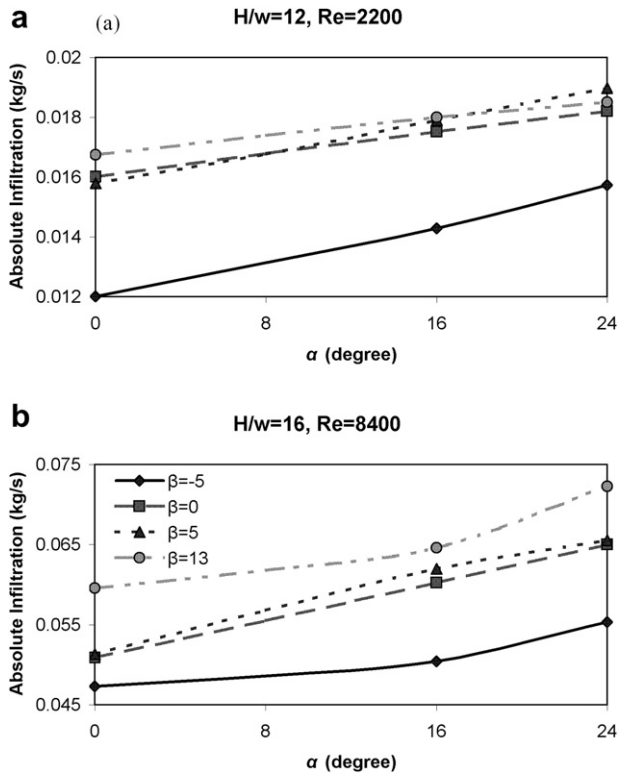

Fig. 5. Effects of offset and throw angles on infiltration at different *H/w* and *Re*, and *K* = 0 [3].
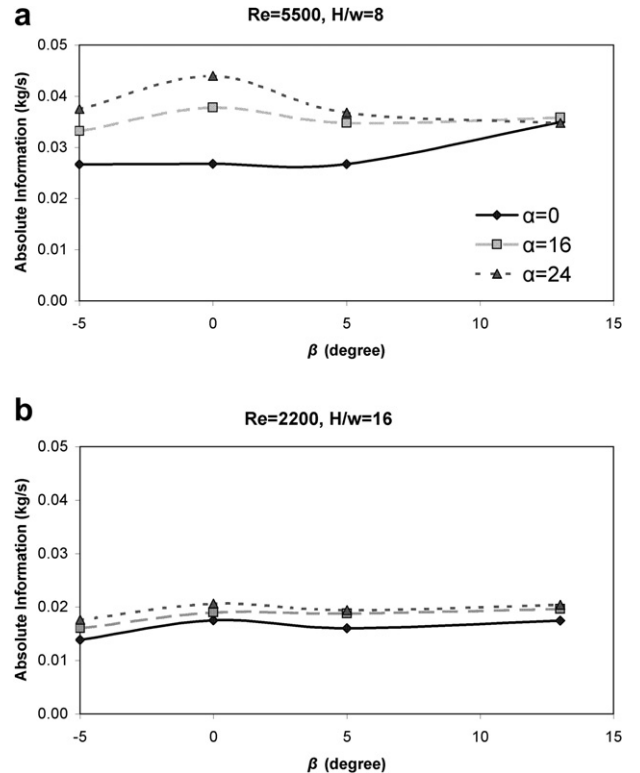

Fig. 6. Effects of throw and offset angles on infiltration at different *Re* and *H/w*, and *K* = 0 [3].
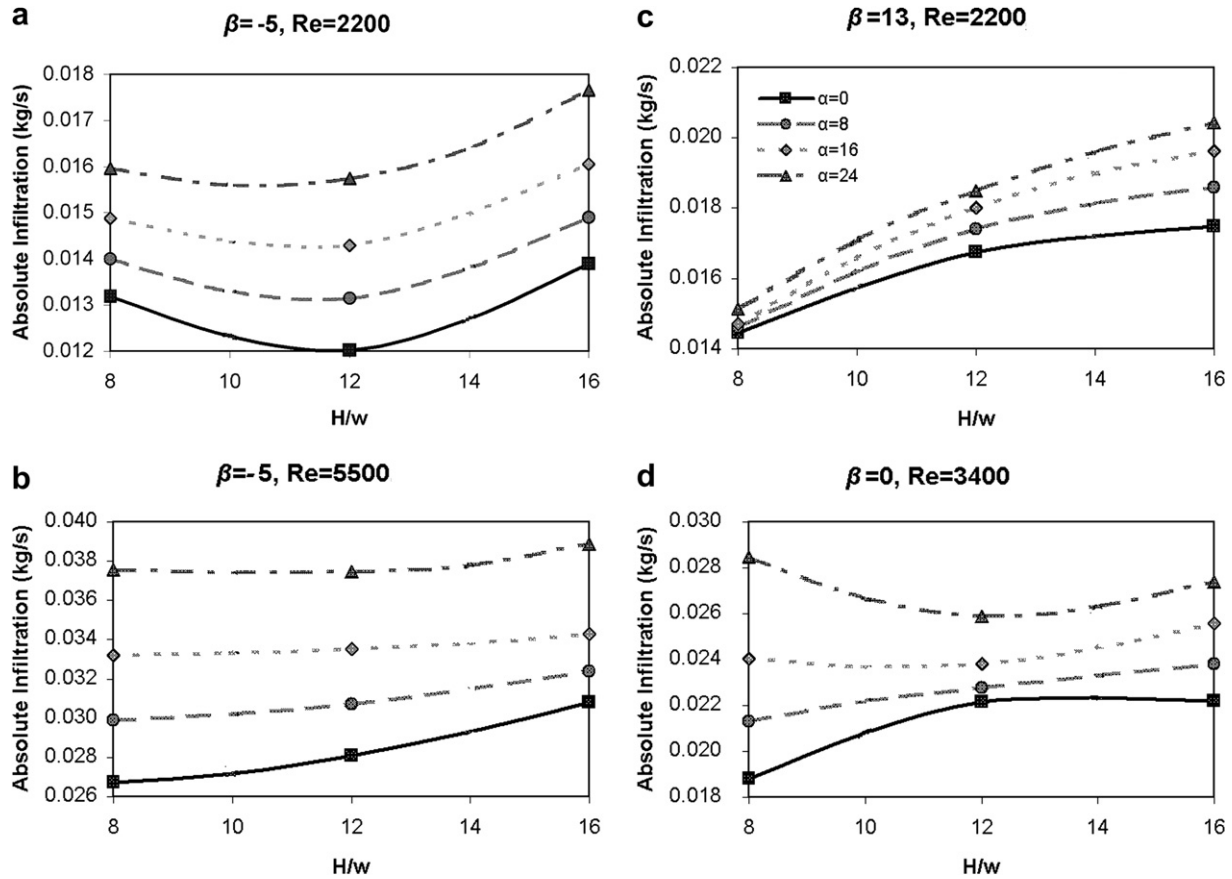
Fig. 7. Effects of opening height and offset angle, at different values of β and Re, and $K = 0$ [3].

3.2. Medium-low cross flow from back panel

At the medium-low values of K (i.e. at $k_1 = 0.35 \pm 0.03$), the total flow rate at the return was increased with respect to the cases with $K = 0$ in order to compensate the flow that exits from the back panel rather the *DAG*. However, the Reynolds numbers at the *DAG* are somewhat different (but not very much) from those of $K = 0$, and all fall within the range of Reynolds numbers to be investigated in this study. This difference is due to the changes in the pressure drop within the reconfigured simulator and display case prototype. At $K = k_1$, the values of Reynolds numbers at the *DAG* for different cases are 1550, 2800, 4900 and 8100.

Some of the results are depicted in Fig. 8. The observation that is common in all the cases at $K = k_1$ is that the infiltration rate at three β values of $-5°, 0°, 5°$ (excluding momentarily the case of $\beta = 13°$) is always the highest at $\beta = -5°$ (in spite of the zero back panel flow configuration in which the least infiltration occurred). This highest value at $\beta = -5°$ may be caused by two possibilities: the first possibility is that the jet interferes with, and partially impinges on the shelves, after which the agitation and instability of the flow are enhanced in the jet region and the mixing of outside air with the jet increases. The second possibility is that at this negative throw angle, a partial counter-flow is caused due to the component of the jet flow that is against the back panel flow. This in turn will augment turbulence, which can: 1) be transported to the outer edge of the air curtain jet and then; 2) increases the mixing of the jet with the outside air and subsequently; 3) results in greater infiltration rate.

However, comparing the results of $K = 0$ and k_1 indicates that at $\beta = -5°$, the infiltration is minimum in the former in contrast to the results of the latter. This confirms that despite the lack of outward

pushing force of the jet by the back panel cross flow, which could help prevent the jet hitting the shelves, at $\beta = -5°$ the minimum infiltration is achieved at $K = 0$. This probably demonstrates that disturbance caused by the *jet-back panel* counter flow near the shelves has a more determinative role in the increase of infiltration.

The throw angle $\beta = 13°$ was not compared with the other angles, as it shows different variations from one configuration to the other. Comparing figure b with figures a and c (all which are at the highest Reynolds number) indicates that only at $H/w = 12$, the infiltration associated with $\beta = 13°$ is higher than those of the other throw angles. This can be explained by knowing that because $H/w = 8$ (in Fig. 8a) is a non-dimensional height at which the smallest proximity of the *RAG* to *DAG* occurs, regardless of how fast the jet exits from the nozzle, the *RAG* can influence the jet relatively faster than the cases with larger heights; as a result, the *RAG* in case $H/w = 8$ can better deflect the jet toward itself, and consequently form a more protective air curtain (as long as forceful impingement does not occur). Consequently, a lower infiltration may be achieved. When the height is increased to $H/w = 12$, influence of the *RAG* on the exit jet is diminished. Thus, the jet with the initial throw angle of $13°$ has more chance to escape that part of the flow field that the *RAG* can influence strongly. So, infiltration increases. When the height increases further to $H/w = 16$ (the longest height in this work), the overall travel distance and travel time from *DAG* to *RAG* increases for the jet. In this case, the jet can achieve distance from the *RAG* similar to the case of $H/w = 12$, but at the same distances from the *RAG*, the flow elements in the $H/w = 16$ case will have lower momentum than the $H/w = 12$ case, and make it easier for the flow elements to be drawn by the *RAG*. This will bring about less infiltration for $H/w = 16$ at $\beta = 13°$, nevertheless, its infiltration at this angle still will be higher than those at $\beta = 0°$ and $5°$ unlike
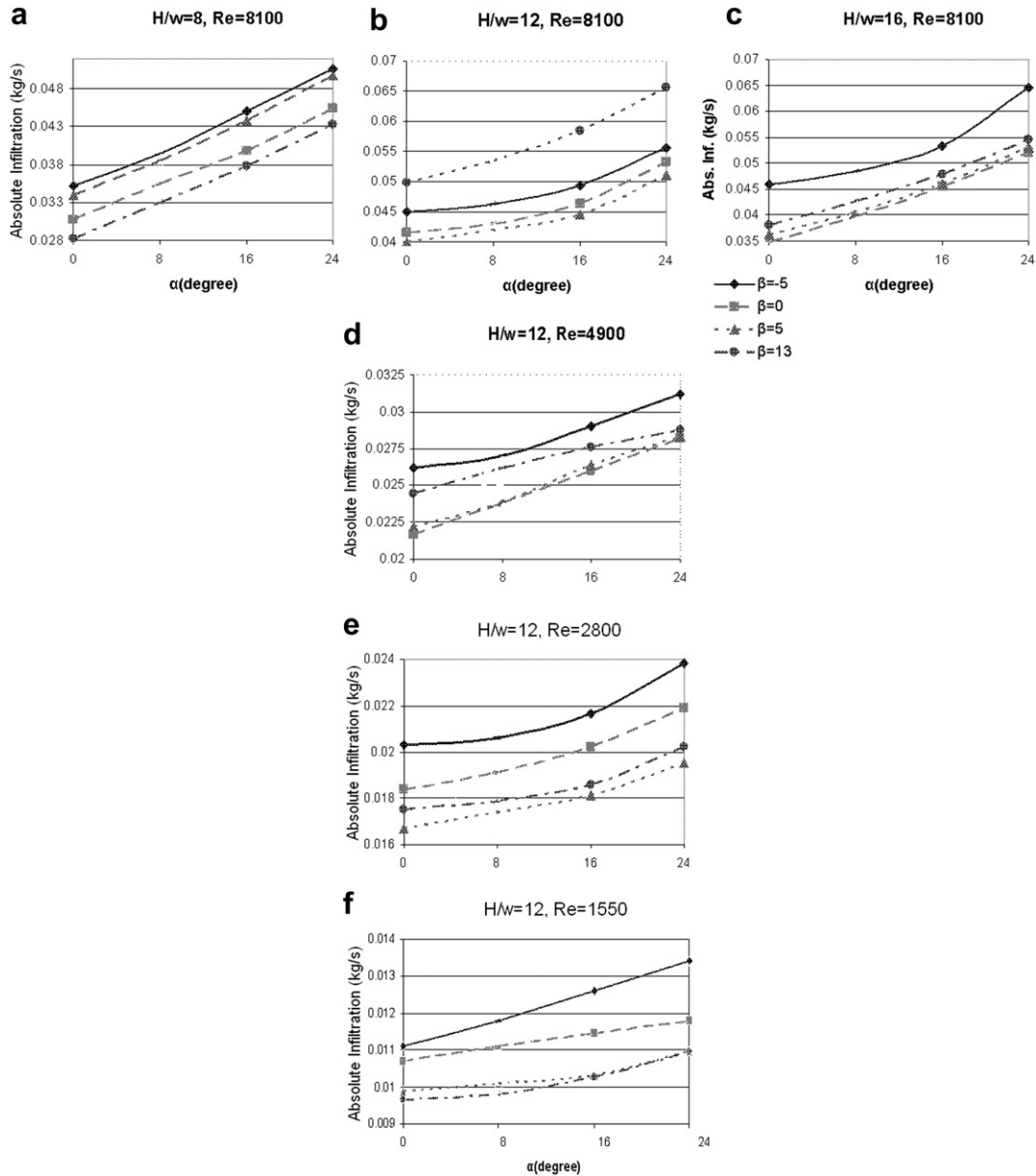
Fig. 8. Effects of α and β on infiltration at different values of H/w and Re, and $K = k_1$.

$H/w = 8$. It should be mentioned that in $H/w = 16$, one may be concerned about the integrity of the air curtain jet being compromised due to the longest jet path, and possibly a great deal of momentum loss, an increase of jet turbulence, and consequently an increase of infiltration. However, the same conclusion may not be made in this air curtain jet-cavity problem because the air curtain jet in this case is more complex than a simple free jet due to the presence of the sink of flow, confinement by cavity boundaries, and interference of the back panel cross flow and the shelves.

The above-mentioned variation of the infiltration with height motivates us to look into the infiltration at other Reynolds numbers as well. However, at $H/w = 8$ and 16 the results at different Reynolds numbers are similar in trend to their counterparts at $Re = 8100$ (i.e. those shown in Fig. 8a and c, respectively), but not for those of $H/w = 12$ (Fig. 8b, d–f). These figures show that the infiltration at $\beta = 13°$ decreases with a decrease in the Reynolds number, which indicates that at smaller Re's (at least in the range of the current study) the discharged jet flow can be more easily deflected toward the RAG, and also the lower turbulence associated

with smaller Reynolds numbers jets help the jet maintain its integrity. The minimum infiltration between $\beta = 0°$ and 5° is interchangeable, but that infiltration always falls between two extreme cases that occur at $\beta = -5°$ and 13°.

Fig. 9 shows that at $K = k_1$, similar to $K = 0$, the infiltration changes linearly or almost linearly with the Reynolds number.

3.3. Medium-hi cross flow from back panel

At the medium high values of K (i.e. at $k_2 = 0.55 \pm 0.03$), the Reynolds numbers at the DAG are also somewhat different from those of $K = 0$ and k_1, but they are not very different and all fall within the range of the Reynolds numbers intended to be investigated in this study. At $K = k_2$ the Reynolds numbers at the DAG are 2100, 3750, 4950 and 7150. The interesting finding in this case is that, unlike the medium-low values of K (i.e. $= k_1$) at which at $\beta = -5°$ almost always the greatest infiltration was produced (except in the case of Fig. 8b), infiltration is always minimum at this angle for $K = k_2$. Fig. 10 shows two sets of sampled data
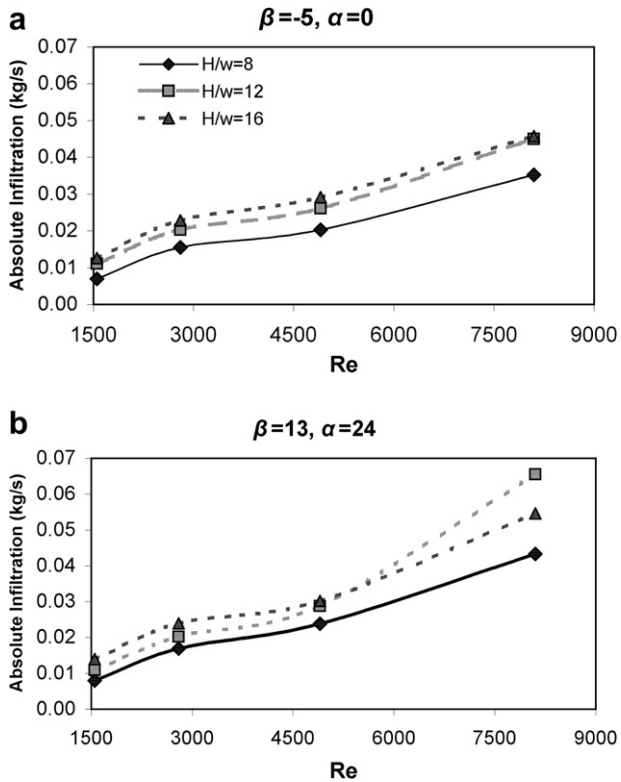
Fig. 9. Effects of *Re* and *H/w* on infiltration at different values of α and β, and $K = k_1$.

representing the entire data set. It is evident that even with greater interference of the jet and the back panel flow due to the larger flows from the back, the back panel flow pushes the jet outward. Especially when $\beta = -5°$, the cross flow better deflects the air curtain jet from the state of impingement on the shelves to a state at which the air curtain jet moves toward the return passage. This will help reduce infiltration at this angle.

The other difference between these two groups of data is that the largest value of infiltration takes place at $\beta = 13°$ for $K = k_2$. This indicates that the latter state of pushing the air curtain outward does not necessarily always help reduce the infiltration. Apparently, the increase of the back panel flow rate from k_1 to k_2 further pushes the air curtain jet away from the display case. As was explained above, this will result either in no impingement or weaker impingement of the jet on the shelves at smaller throw angles. As a consequence, the turbulence in these cases will be smaller; that in turn can potentially generate smaller infiltration. Nonetheless, when $\beta = 13°$, the jet is already directed almost outward and is still pushed further outward by the back panel cross flow, outside the influence region of the suction of the *RAG*. This will diminish the integrity of the air curtain jet and will cause an increase in infiltration. After examining the previously-mentioned behavior of $\beta = -5°$, one may anticipate that $\beta = 0°$ causes the second smallest infiltration. However, looking again at Fig. 10, the results indicate that in Fig. 10a (and some other configurations) $\beta = 0°$ results in the smallest infiltration, while in some other configurations, such as that shown in Fig. 10b, $\beta = 5°$ can produce lesser infiltration than $\beta = 0°$. In case *a*, the jet flow will have relatively larger momentum between the *DAG* and *RAG* than the other case; therefore, the jet is relatively more resilient against the impact by the cross flow. It is speculated that in the configurations that the jets lose more
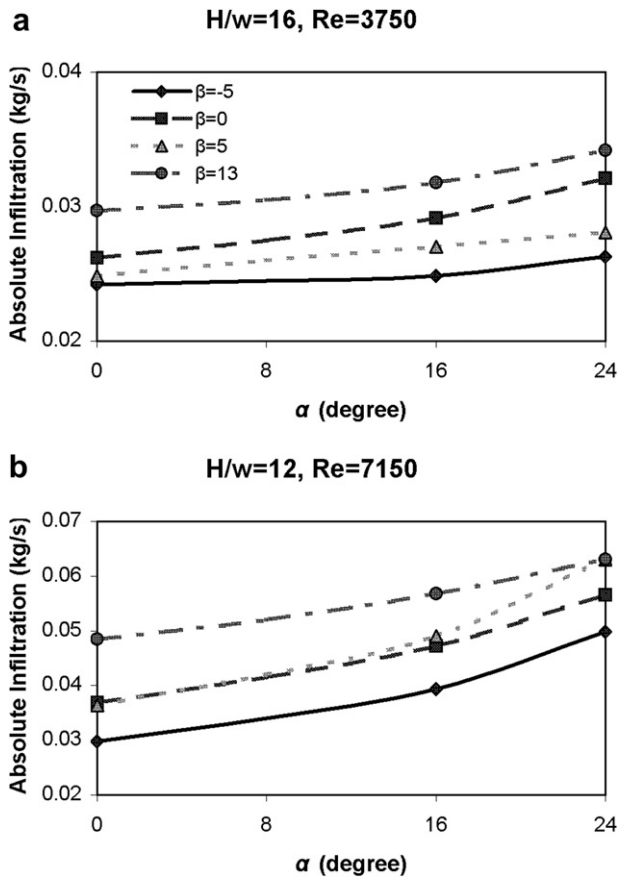

Fig. 10. Effects of α and β on infiltration at different values of *H/w* and *Re*, and $K = k_2$.
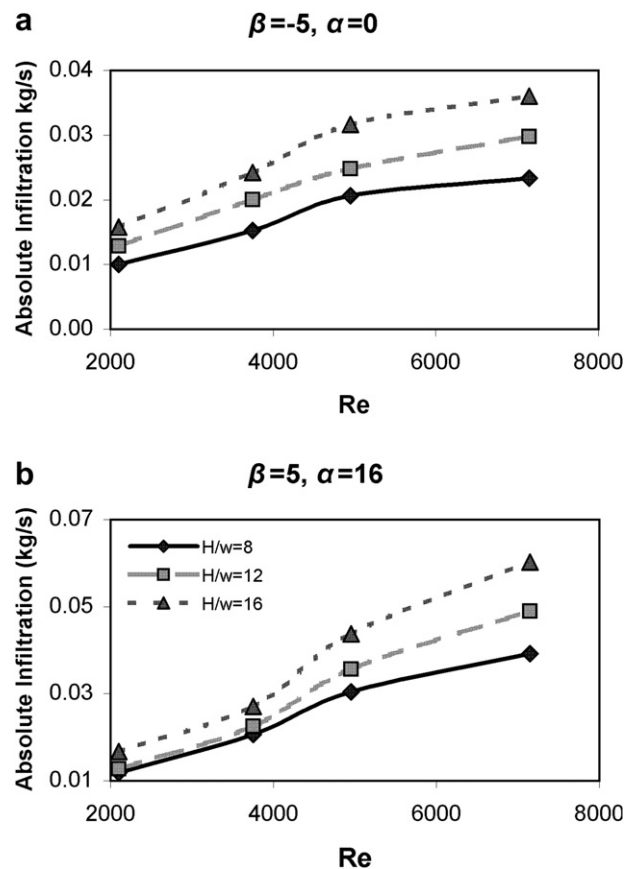

Fig. 11. Effects of *Re* and *H/w* on infiltration at different values of α and β, and $K = k_2$.

momentum when traveling from the *DAG* to the *RAG*, the jet with $\beta = 0°$ will experience an almost 90° transverse impact by the cross flow from the back panel.

This will yield a more intense impact and more agitated flow than the cases with the outward tilted jet (i.e. at $\beta = 5°$). In this situation the initially horizontal back panel flow will have more time to change its path downward and reduce the impact angle before approaching the jet. Similar to the other cases of back panel flow rate ratios, here too, the infiltration increases linearly (or almost linearly) with the Reynolds number (Fig. 11).

3.4. Zero DAG flow

The highest level of the back panel flow ratio is when the flow at the *DAG* is completely blocked and all the flow drawn through the *RAG* is discharged from the back panel perforated plate, $K = 1$.
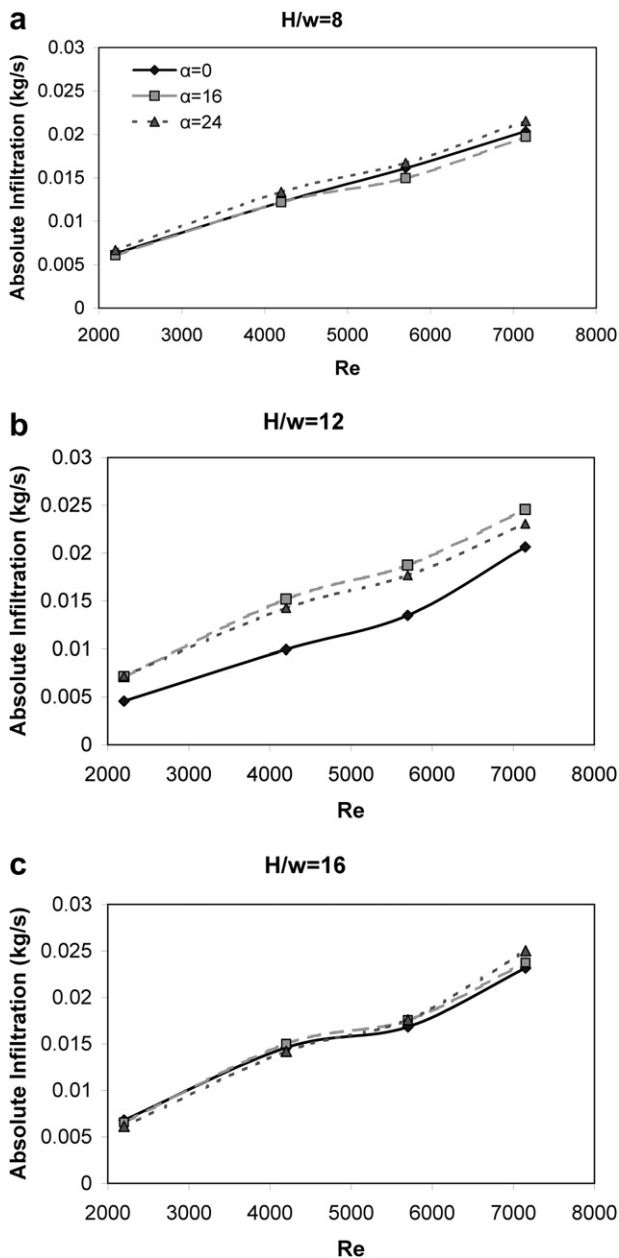
Obviously there is no effect of change of β in this case as there is no flow initiated from the *DAG*. Fig. 12 presents the infiltration results at different H/w values. Similar to the other cases, in this case too, the absolute infiltration rate increases with the Reynolds number. Additionally, the infiltration and Reynolds number are nearly linearly related. Subsequently, one can assume there will be smaller infiltration rates when the distance between the back panel and the *RAG* (and therefore α) is smaller. But the results explain that this takes place only at $H/w = 12$. Interestingly, at $H/w = 8$ and 16, no significant differences were found between the infiltration values with changes in offset angle (α) values. This shows that only at $H/w = 12$ can one find the optimum values of infiltration with respect to the offset angle. When $H/w = 8$ and 16, because the same infiltration rate is yield at different offset angles, system designers can enjoy larger horizontal space within the display cases without using extra energy initiated from infiltration.

Similar to the results of other back panel flow rate ratios, absolute infiltration changes linearly, or almost linearly, with offset angle. Results in Fig. 13 confirm that at $\alpha = 0°$, a minimum infiltration can be found around $H/w = 12$ when $K = 1$. Also, the average infiltration at $\alpha = 16°$ is almost identical to that of $\alpha = 24°$. However, at $H/w = 8$ and 16 infiltration is almost equal in all offset angles. The results of infiltration at different K ratios were not compared directly (i.e. plots of infiltration at the same H/w, β, α for different K's were not produced), because at different values of H/w, β, and α, the order that the minimum-to-maximum values of infiltration is interchanged depends on the values of the above variables. For instance, at $(H/w, \beta, \alpha)_1$, $K = 0$ results in the minimum infiltration but at $(H/w, \beta, \alpha)_2$, $K = k_2$ will yield the minimum.
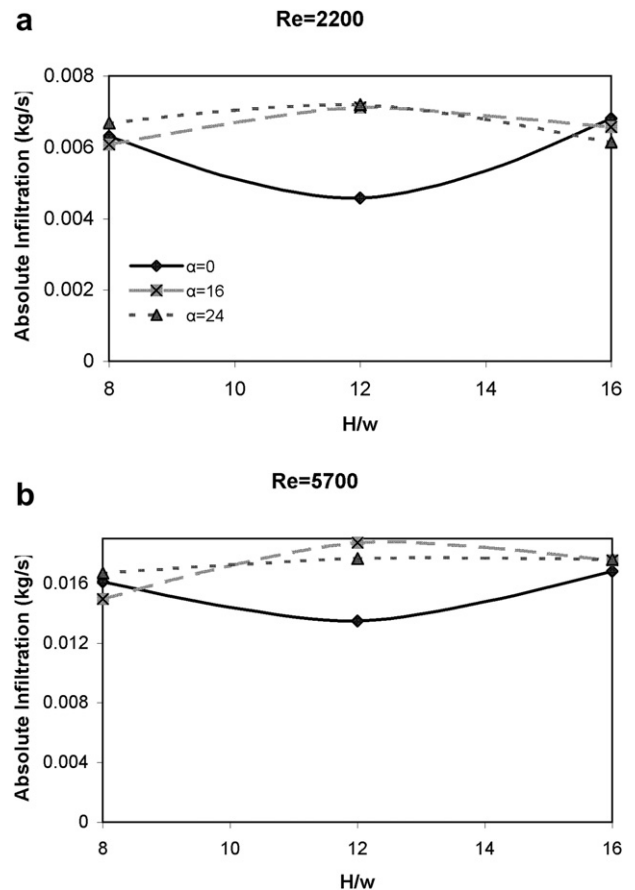
Fig. 12. Effect of *Re* and α on infiltration at different values of *H/w*, and $K = 1$.

Fig. 13. Effect of *H/w* and α on infiltration at different *Re* values, and $K = 1$.

Table 2
Minimum and maximum values of a) absolute, b) non-dimensional infiltration rates (courtesy of California Energy Commission [12]).

(a)			Infiltrated air (kg/s)	Corresponding N.I.R.	β	H/w	α	Re_{DAG} (± 200)	K
1	Absolute	Min	0.0046	10.2%	0°	12	0°	2200	1
2	values	Max	0.073	42.3%	13°	16	24°	8400	0

(b)			N.I.R.	Corresponding infiltrated air (kg/s)	β	H/w	α	Re_{DAG} (± 200)	K
1	N.I.R.	Min	8.37%	0.0094	5°	8	0°	5500	0.62
2	values	Max	46.20%	0.0207	0°	16	24°	2200	0

Indeed, the designers of such systems should obtain identical *N.I.R.*s if the same *Re*, *H/w*, β, α and *K*, presented in Table 2a, are used, and if the turbulence intensity of the velocity of the air curtain jet at the *DAG* are the same and velocity profile shapes are similar. The minimum and maximum values of *N.I.R.* have been shown in Table 2b. As was explained previously, one may infer that *N.I.R.* is indicative of the efficiency of a display case. A display case is more efficient (as regards infiltration) than a similar display case with the same total flow rate if it brings about less *N.I.R.* It was observed that even in cases where the air curtain is generated with smaller Reynolds numbers (or smaller total flow rates), the *N.I.R.*'s were significantly greater than those of some of the higher Reynolds numbers. Thus, it is not necessarily correct to conclude that at higher-speed operations the *N.I.R.* will be greater. For example, case 3 in Table 2b yields the minimum global *N.I.R.* (8.37%) operates at higher speed (*Re* = 5500) than case number 4 (*Re* = 2200), which causes maximum global *N.I.R.* With smaller *N.I.R.*, however, the former case (although it has the minimum *N.I.R.*) infiltrates more outside air mass than the latter case (1.246 vs. 2.734 L/min).

The results of this table show that drastic improvement to the air curtain performance, i.e. reducing the *absolute* infiltration rate, can be readily achieved by altering one or more independent non-dimensional variables, even if *N.I.R.* is compromised.

As explained above, it was observed from the pool of infiltration data that the infiltration is a strong function of all the variables. However, infiltration did not show a well-defined pattern of change with each of those variables. For this reason it may not be possible to draw a universal conclusion about the behavior of infiltration rate with respect to each individual variable. There are hundreds of data points that fall between the above minimum and maximums. Since in this work infiltration is dependent on five variables: *Re*, *H/w*, β, α and *K*, it will be difficult to interpolate the data for each particular test condition. For resolving this problem, a Neural Network program that was developed by Prismitech LLC, was used to perform interpolation on multi-dimensional surfaces. Using this tool, one can fix some variables and vary others in order to find a smaller or the smallest possible infiltration rates.

4. Conclusions

Tracer gas method has proven to be an efficient and accurate method for measuring the infiltration rate in open refrigerated display cases. From our experiments, it was found that the amount of infiltration significantly depends on the geometrical configuration of the system, and also the Reynolds number of the jet at the nozzle exit when the turbulence intensity is almost fixed at the air curtain discharge. It was observed that it is difficult to identify a unique trend of change in infiltration for every independent variable. However, some of the variables showed relatively well-defined trends while others did not; in the entire back panel cross flow ratios, the absolute infiltration always increased with

increase of Reynolds number with a linear or nearly linear trend. On the other hand, the non-dimensional infiltration rate (*N.I.R.*) showed an opposite behavior, i.e. *N.I.R.* usually decreased with an increase of the Reynolds number and with a non-linear trend. Similar to the effect of *Re* on absolute infiltration rate, an increase of offset angle in most cases enhanced the infiltration rate in the entire range of the variables tested in the current study. In the same fashion, linear or quasi-linear relationships were seen between offset angle and absolute infiltration.

No robust relationships were found between throw angle and infiltration rate, or between height of ORVDC and infiltration. It was observed that by varying each of the above two variables, one could find an extreme point for absolute infiltration. Moreover, the cross flow from the back panel usually reduced the infiltration at smaller offset angles and smaller travel distances, as well as at smaller Reynolds numbers. Overall, the results indicated that infiltration not only is dependent on the values of *H/w* and β, but is also very sensitive to the combination of these variables with the others, more so than *Re* and α. For example, in some cases the minimum infiltrations occurred at $\beta = -5°$ when $K = 0$, and in other cases such as when $K = k_1$, it could occur at $\beta = +5°$. The change of β with respect to α not only can affect the infiltration by aiming the jet at or diverting it from the return passage, it may also have a secondary effect in the form of impingement of the jet on the lowest level of the *ORVDC*. That is, if $\beta < \alpha$, the impingement may occur. Depending on the other variables such as height, Reynolds number and the ratio of the back panel flow to the total flow, the severity of the impingement and subsequent flow disturbance and infiltration may differ. Finally, the results that we have obtained so far will help designers and manufacturers of open refrigerated display cases design more cost-efficient and energy-friendly systems by making minor changes that can save U.S. supermarkets up to $100 million/year [17].

Acknowledgements

References

[1] Oakridge National Lab, ORNL/TM-2004/292, (2004).
[2] R.H. Howell, P. Adams 596RP, in: Effects of Indoor Space Conditions on Refrigerated Display Case Performance, ASHRAE, 1991.
[3] M. Amin, D. Dabiri, H.K. Navaz, Experimental investigation of the effect of various parameters on the infiltration rates of single band open vertical refrigerated display cases with zero back panel flow, ASHRAE Transactions 115 (2009–1) 255–265.
[4] M. Amin, D. Dabiri, Effect of boundary condition at nozzle discharge on the development and entrainment of free rectangular jets, International Journal of Numerical Methods for Heat & Fluid Flow, in preparation.
[5] H.K. Navaz, M. Amin, S.C. Rasipuram, R. Faramarzi, Jet entrainment minimization in air curtain of open refrigerated display cases, International Journal of Numerical Methods for Heat and Fluid Flow 6 (2006) 417–430.
[6] F.C. Hayes, W.F. Stockers, Design data for air curtains, ASHRAE Transactions (1969) 153–167.
[7] O. Rouaud, M. Havet, Behavior of an air curtain subjected to transversal pressure variations, Journal of Environmental Engineering-Asce 132 (2006) 263–270.
[8] Y.G. Chen, Parametric evaluation of refrigerated air curtains for thermal insulation, International Journal of Thermal Sciences 48 (2009) 1988–1996.
[9] B. Field, R. Kalluri, E. Loth, in: PIV Investigation of Air-curtain Entrainment in Open Display Cases, IIF-II-Commission D1/B1, Urbana, IL, 2002.
[10] M. Amin, D. Dabiri, H.K. Navaz, Air Curtain performance studies in open vertical refrigerated display cases, in: Heat Transfer 2008 Conference, Slovenia, 2008.
[11] H.K. Navaz, M. Amin, D. Dabiri, R. Faramarzi, Past, present, and future research towards air curtain performance optimization, ASHRAE Transactions 111 (2005) 1083–1088.

[12] R. Faramarzi, M. Amin, H.K. Navaz, D. Dabiri, D. Rauss, R. Sarhadian, Air Curtain Stability and Effectiveness in Open Vertical Refrigerated Display Cases. California Energy Commission, 2008.

[13] H.K. Navaz, R. Faramarzi, D. Dabiri, M. Gharib, D. Modarress, The application of advanced methods in analyzing the performance of the air curtain in a refrigerated display case, Journal of Fluids Engineering 124 (2002) 756–764.

[14] G. Rigot, Meubles et vitrines frigorifiques (1990) Pyc ed.

[15] M. Amin, D. Dabiri, H.K. Navaz, Tracer gas technique: a new approach for steady state infiltration rate measurement of open refrigerated display cases, Journal of Food Engineering 92 (2009–2) 172–181.

[16] H.K. Navaz, R. Faramarzi, Advanced supermarket display case workshop, ASHRAE winter meeting, (2004).

[17] California Energy Commission (CEC) & Southern California Edison (SCE) Co., Private Communication (2003).